An Analysis on Natural Image Small Patches

Shengxiang Xia
School of Science,
Shandong Jianzhu University,
Jinan 250101 P.R.China

Wen Wang
School of Science,
Shandong Jianzhu University,
Jinan 250101 P.R.China

Di Liang
School of Science,
Shandong Jianzhu University,
Jinan 250101 P.R.China

***Abstract*—The method of computational homology is used to analyze natural image 8×8 and 9×9-patches locally. Our experimental results show that there exist subspaces of the spaces of 8×8 and 9×9-patches that are topologically equivalent to a circle and a Klein bottle respectively. These extend the results of the paper "on the local behavior of spaces of natural images." To the larger patches. The Klein bottle feature of natural image patches can be used in image compression.**

***Keywords*—natural image analysis; persistent homology; high-contrast patches; Klein bottle; barcode**

I. Introduction

Many results on statistics of images were obtained in the recent years [1], [2], [3]. Lee, Pedersen, Mumford [3] discuss the distributions of 3×3 image patches, they found that the majority of high-contrast 3×3 patches concentrate near A circle. Carlsson, Ishkanov, de Silva, and Zomorodian [4] analyze 3×3 natural image patches; they find a high density the subset is called the primary circle and prove that there exists the large 2-dimensional subset with the topology of a Klein bottle Which includes the primary circle. In [5], we showed that 4×4, 5×5, 6×6 and 7×7 natural image patches have the circle behavior.

In this paper, we utilize the methods of the paper [4] to study the structure of $n\times n$ high-contrast natural image patches for the cases n=8 and n=9. In particular, we find the largest 2-Dimensional subspace of each case, whose topology is that of a Klein bottle. The results of the paper enlarge the results of [4] To 8×8 and 9×9 patches. The Klein bottle feature of image patches can be used in techniques of image compression [4], [6]. The data sets used in this paper were chosen from INRIA Holidays dataset [7], which are different from that of the paper [4].

II. The Data Sets of Natural Image Patches

As the dimensional problem of the data, it is very difficult To directly analyze the pixel distribution of images. We divide each natural image into small $n\times n$-patches, and consider each patch as an n^2-dimension vector, we study the topology of the space of $n \times n$-patches for sufficiently small n, here we study the cases of n=8, 9.

We sample data sets of high-contrast 8×8 and 9×9 Patches from 550 sampled natural images in INRIA Holidays dataset [7]. Each data set consists of about $55 \cdot 10^5$ high-Contrast log patches. INRIA Holidays dataset is available at http://lear.inrialpes.fr/%7ejegou/data.php. Fig.1 has two samples.

Our main spaces X_8 and X_9 are sets of 8×8 and 9×9 Patches of high contrast created by the following steps. The routine handled here is similar to [3], [4], [8].

Step 1. Sample 550 images from INRIA Holidays dataset.

Step 2. Using MATLAB function rgb2gray to compute the intensity at each pixel for each image.

Step 3. We randomly select 5000 8×8 and 9×9 patches from each image.

Step 4. We treat each patch as an n^2-dimensional vector, and take the logarithm of each coordinate.

Step 5. For any vector $\mathbf{x}$=$(x_1, x_2, ..., x_n)$, we calculate the D-norm: $\| \mathbf{x} \|_D$. Two coordinates of $\mathbf{x}$ are neighbors, expressed by $i \sim j$, if the corresponding pixels in the $n \times n$ patch are adjacent. The formula of D-norm is: $\| \mathbf{x} \|_D = \sqrt{\sum_{i\sim j}(x_i - x_j)^2}$.

Step 6. We select the patches which have a D-norm in the top t percent in each image. We take t = 20%, as done in [3], [4], [8].

Step 7. Subtract an average of all coordinates from each coordinate.

Step 8. We map X_8 (X_9) into a unit sphere by dividing each vector with its Euclidean norm. We do not translate to the DCT basis for convenience.

Step 9. We randomly select 50,000 points from X_8 and X_9 for computational convenience, the subspaces of X_8 and X_9 are indicated by $\bar{X}_8$ and $\bar{X}_9$ respectively.

III. Computational Method

For determining topological features of an underlying space by sampled finite points, the computing method used in this paper is persistent homology, which is set up by Edelsbrunner, Letscher, and Zomorodian [9] and distilled by Carlsson and Zomorodian [10]. To apply persistent homology, we firstly build lazy witness complexes for a sampled point set P from underlying space X.

For a point cloud P, a landmark subset L, for all $p \in P$. Let $t(p)$ be the distance p to the closest landmark point. The lazy witness complex $LW(P, L, \epsilon)$ is formulated as follows: (i) the vertex set is L; (ii) for vertices a and b, edge [ab] is in $LW(P, L, \epsilon)$ if there is a witness point $p \in P$ such that

$$\max\{d(a, p), d(b, p)\} \leq \epsilon + t(p);$$

(iii) a higher dimensional simplex is in $LW(P, L, \epsilon)$ if all of its edges are.

Fig. 1. Samples from INRIA Holidays dataset

The most important parameter in a sequence of lazy witness complexes is ϵ, but there is no an optimal value of ϵ without prior information of the underlying space, we do not know how To pick the value of ϵ. However, using the Javaplex package developed by Adam and Tausz [12], we can compute the Betti numbers in an interval of ϵ and explain the result by a Betti barcode. The instinctive explanation is that long intervals accord to actual topological features of the underlying space while short ones are explained as noise.

To uncover the topological features of our spaces X_8 and X_9, we use the different core subsets of X_8 and X_9. We evaluate the local density of the space at a point by its the nearest neighbor. For $y \in X$ and $k > 0$, let $\rho_k(y) = \mid y - y_k \mid$, here y_k is the kth nearest neighbor of y. The larger k-Values contribute more global estimations, while small k-Values result in local density estimates. For a given k, we arrange the points of X by descending density; we pick the points with densities in the top p percent, written as $X(k,p)$. The core subset $X(k,p)$ possibly give important topological information, which may be disappeared for all the points of X.

Here we examine core subsets $\bar{X}_n(k,p)$ of $\bar{X}_n$ for $n = 8, 9$. Core subsets have two parameters k and p, they demonstrate some topological features of their underlying space for k and p with suitable values.

IV. Results for $\bar{X}_8(k,p)$ and $\bar{X}_9(k,p)$

The authors of the paper [4] applied persistent homology to detect the topologies of high-density subsets of natural image patches. They discovered that the topology of the core sets vary from a circle to a 3-circle model as decreasing of Density estimator k. In this paper, we use INRIA Holidays data set, which is other than that of the paper [4], to prove experimentally that some core sets of X_8 and X_9 possess the similar results as above.

We take the core subsets $\bar{X}_8(300,20)$, $\bar{X}_9(300,20)$, and calculate the barcodes by Javaplex software, their sample barcode plots are displayed in Fig.2, Fig.2 separately. In Fig.2, Fig.3, there exist a single long line of $Betti_0$ and a single long $Betti_1$ line (i.e. $\beta_0 = 1$ and $\beta_1 = 1$), which means that they have the topology of a circle. When we project core sets onto some plane, their circle feature is visible in Fig.4 and Fig.5. Choosing different landmark points, we run many times experiments on $\bar{X}_8(300,20)$, $\bar{X}_9(300,20)$, and the results are very steady.

For 8×8 and 9×9 patches, there are much different cores subsets of $\bar{X}_8$ and $\bar{X}_9$, if we take proper values of parameters k and p, the core sets also have the topology of a circle. For $\bar{X}_8(100,20)$, $\bar{X}_8(200,20)$, $\bar{X}_9(100,20)$ and $\bar{X}_9(200,20)$, We ran many trials and found that they have the topology of a circle and the results to be robust.

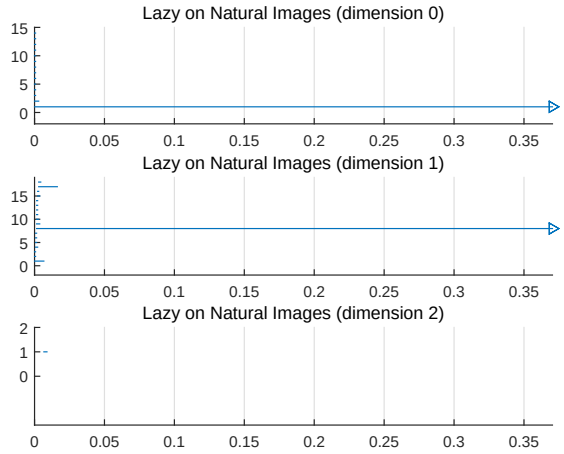

Fig. 2. PLEX results for $\bar{X}_8(300,20)$

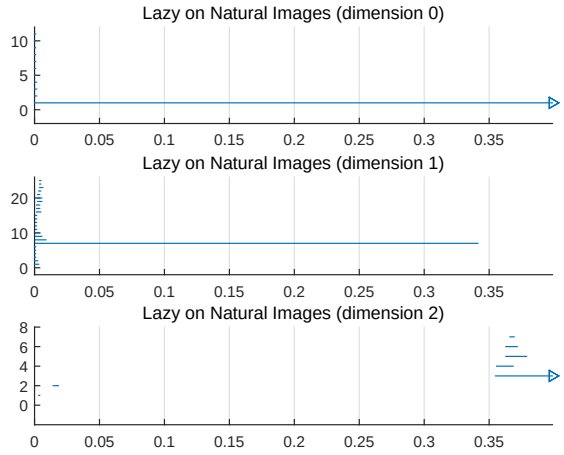

Fig. 3. PLEX results for $\bar{X}_9(300,20)$

When we consider the core subsets $\bar{X}_8(15,20)$, $\bar{X}_9(15,20)$, and calculate the barcodes, their sample barcode plots are shown in Fig.6, Fig.7 separately. In Fig.6 (Fig.7), there are a single long line of $Betti_0$ and five long $Betti_1$ line for ϵ from 0.06 to 0.18 (from 0.05 to 0.19), which shows that they have the topology of three circle model [4] (Fig.8), that is, Betti numbers $\beta_0 = 1$ and $\beta_1 = 5$.

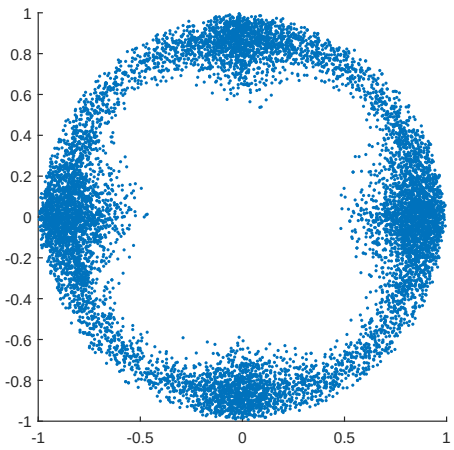

Fig. 4. Projection of $\bar{X}_8(300, 20)$ onto a plane

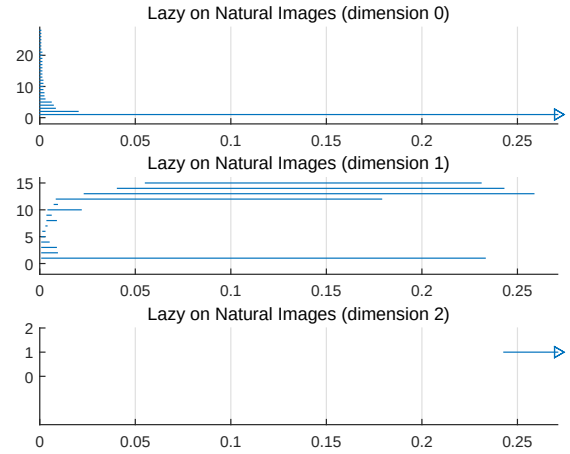

Fig. 6. PLEX results for $\bar{X}_8(15, 20)$

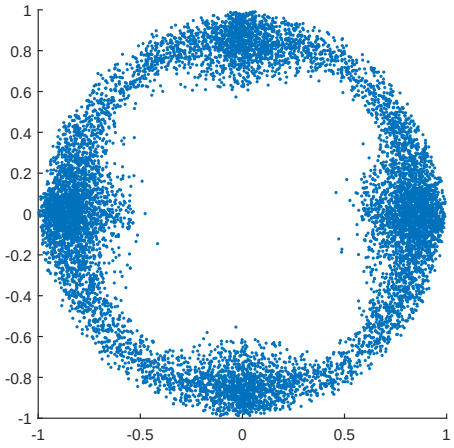

Fig. 5. Projection of $\bar{X}_9(300, 20)$ onto a plane

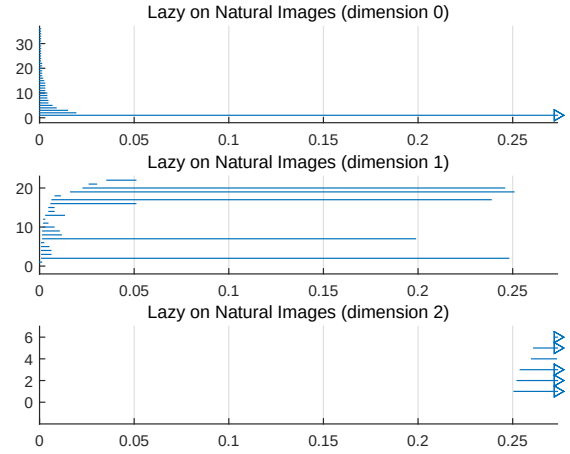

Fig. 7. PLEX results for $\bar{X}_9(15, 20)$

V. Embedding of the Klein Bottle into S^{63} and S^{80}

The Klein bottle is a very important non-orientable surface, it can be sketched by the quotient space of the square $[0, 1] \times [0, 1]$ with sides glued by the relations $(0, y) \sim (1, y)$ for $y \in [0, 1]$ and $(x, 0) \sim (1 - x, 1)$ for $x \in [0, 1]$. To identify the Klein bottle features of subspaces of X_8 and X_9, we embed the Klein bottle into S^{63} and S^{80}, and get another theoretical model of the Klein bottle.

We define the map $g : S^1 \times S^1 \longmapsto \mathcal{P}$ by $(\cos\alpha, \sin\alpha, \cos\beta, \sin\beta) \longmapsto \cos\beta(x\cos\alpha + y\sin\alpha)^2 + \sin\beta(x\cos\alpha + y\sin\alpha)$ ([4]), where $\mathcal{P}$ consists of all functions with the form $\cos\beta(x\cos\alpha + y\sin\alpha)^2 + \sin\beta(x\cos\alpha + y\sin\alpha)$, α, $\beta \in [0, 2\pi]$, it is obvious that g is onto, but not one to one, since the points $(\cos\alpha, \sin\alpha, \cos\beta, \sin\beta)$ and $(-\cos\alpha, -\sin\alpha, \cos\beta, -\sin\beta)$ are mapped to the same function, that is, $(\cos\alpha, \sin\alpha, \cos\beta, \sin\beta) \sim (-\cos\alpha, -\sin\alpha, \cos\beta, -\sin\beta)$ is an equivalent relation, the relation can be rewritten as $(\alpha, \beta) \sim (\pi + \alpha, 2\pi - \beta)$. The space $\mathcal{P}$=im(g) is homeomorphic to $S^1 \times S^1/(\alpha, \beta) \sim (\pi + \alpha, 2\pi - \beta)$, as no other identifications produced by g.

A torus has a similar representation to that of the Klein bottle as glued a square with the opposite edges (Fig.9). The effect of the map g on a torus is displayed in Fig.10. Each half is a representation of the Klein bottle, thus the image of g is homeomorphic to the Klein bottle and so is $\mathcal{P}$ ([4]).

We define a map $h_8 : \mathcal{P} \longmapsto S^{63}$ by a composite of evaluating a polynomial at each point of the plane grid $G_8 = \{-3, -2, -1, 0, 1, 2, 3, 4\} \times \{-3, -2, -1, 0, 1, 2, 3, 4\}$ subtracting the mean and normalizing. In a similar way, we define $h_9 : \mathcal{P} \longmapsto S^{80}$ on the grid $G_9 = \{-4, -3, -2, -1, 0, 1, 2, 3, 4\} \times \{-4, -3, -2, -1, 0, 1, 2, 3, 4\}$. Because continuous 1-1 map on a compact space is a homeomorphism onto its image, as Proved in [4], the images $im(h_8)$ and $im(h_9)$ are homeomorphic to the Klein bottle.

To embed the Klein bottle into into S^{63} and S^{80}, primarily, we uniformly take 200 points ($\{x_1, ..., x_{200}\}$) from the unit circle, all possible tuples (x_i, x_j) produce a point set on the torus $S^1 \times S^1$. Secondly, we map each of the 40000 points into S^{63} and S^{80} through compositions of $h_8 \circ g$ and $h_9 \circ g$ separately,

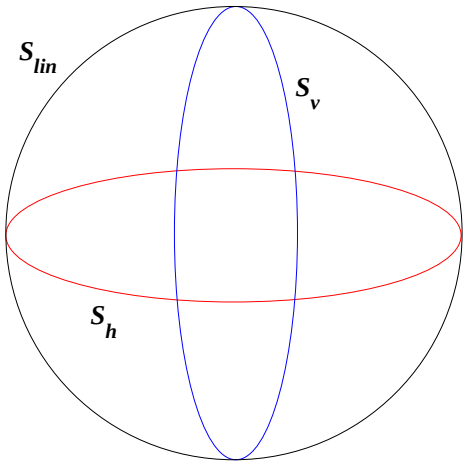

Fig. 8. Three circle model

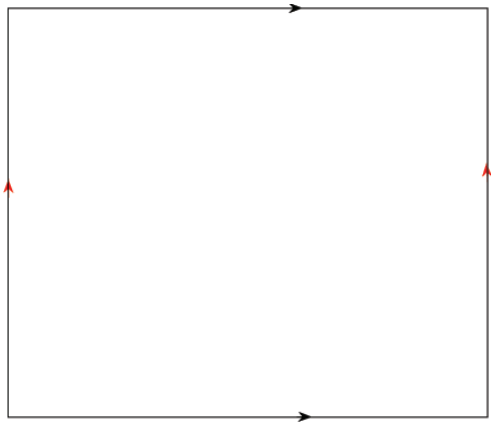

Fig. 9. Denotation of a torus as a quotient space

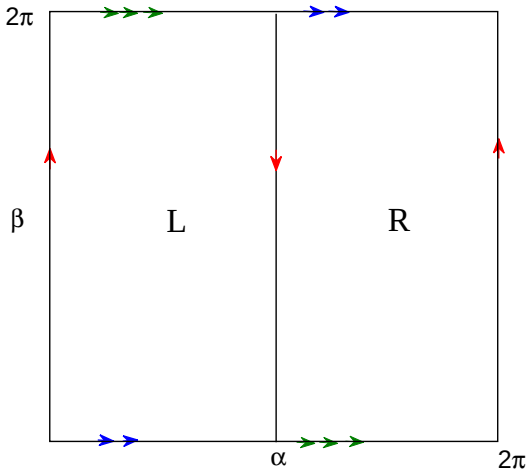

Fig. 10. Klein bottle, the image of the map g

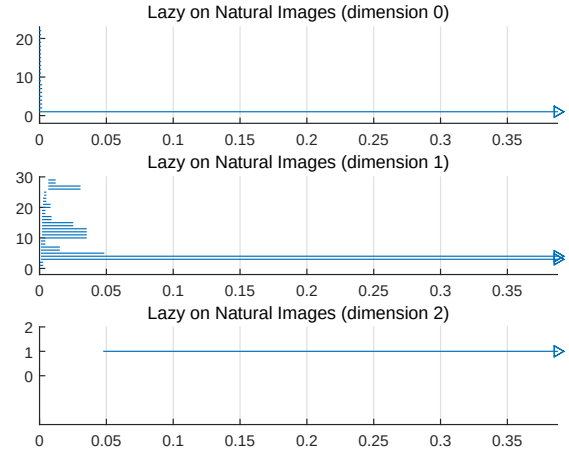

Fig. 11. PLEX result for $K_8(200)$

and the image of the composition is presented by $K_8(200)$ and $K_9(200)$ respectively. Fig.11, Fig.12 display the PLEX results of the spaces $K_8(200)$ and $K_9(200)$ respectively, they provide the Betti numbers $\beta_0 = 1, \beta_1 = 2$ and $\beta_2 = 1$, these are the mod 2 Betti numbers of the Klein bottle. Therefore, $K_8(200)$ ($K_9(200)$) is an appropriate approximation of the Klein bottle in S^{63} (S^{80}).

VI. Results for X_8 and X_9

We have embedded the Klein bottle into S^{63} and S^{80}, and the subspaces $K_8(200)$ and $K_9(200)$ are a proper approximation of the Klein bottle in S^{63} and S^{80} respectively. Applying $K_8(200)$ and $K_9(200)$, we can find subspaces of X_8 and X_9, whose topology is that of the Klein bottle. The constructing process of the subspaces of X_8 and X_9 are as following.

For each point of X_8, we compute the Euclidean distance from the point to point set $K_8(200)$, then we resort points of X_8 according to increasing of their Euclidean distances to $K_8(200)$, then we take the top t percent of the closest distances, and represent the subspace of X_8 as $XP_8(200, t)$. The subspace $XP_9(200, t)$ of X_9 is constructed by a similar way.

To find subspaces of X_8 and X_9 having the topology of the Klein bottle, we take the parameter t=20 we do many experiments on $XP_8(200, 20)$ for the parameter num-landmark-points from 80 to 100 and the result is very stable. Fig.13 displays one PLEX result for $XP_8(200, 20)$, which gives Betti numbers $\beta_0 = 1, \beta_1 = 2$ and $\beta_2 = 1$ for ϵ from 0.019 to 0.059. When taking $t = 25$, the space $XP_8(200, 25)$ experience a topological change. Indeed, we do 50 trials on $XP_8(200, 25)$ for different parameters, where there exist 23 trials whose PLEX results producing the topology of the Klein bottle and most barcode intervals with the homology of the Klein bottle is in very small ranges, the other 27 trials give no the homology of the Klein bottle. Fig.14 gives the Betti numbers of $XP_8(200, 25)$: $\beta_0 = 1, \beta_1 = 2$ and $\beta_2 = 1$ for ϵ from 0.025 to 0.035. The PLEX result Fig.15 of $XP_8(200, 25)$ shows that it has no the Klein bottle's homology. Similarly, we do many experiments on $XP_9(200, 18)$ and $XP_9(200, 23)$ respectively, we discover that the largest subspace of X_9 having the homology of the Klein bottle is about $XP_9(200, 18)$, and the subspace $XP_9(200, 23)$ experiences a topological change. Fig.16 displays one PLEX result for $Xp_9(200, 18)$, which gives $\beta_0 = 1, \beta_1 = 2$ and $\beta_2 = 1$ for ϵ in [0.032, 0.086]. Fig.17 shows $XP_9(200, 23)$ having the Klein bottle feature

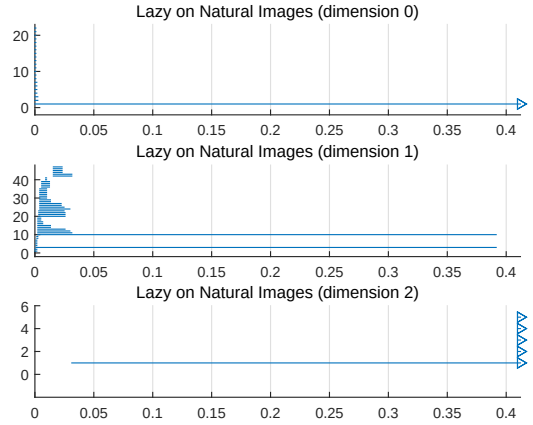

Fig. 12. PLEX result for $K_9(200)$

in a very small range of ϵ values (from 0.014 to 0.033). The PLEX result for $XP_9(200, 23)$ in Fig.18 gives no the Klein bottle feature.

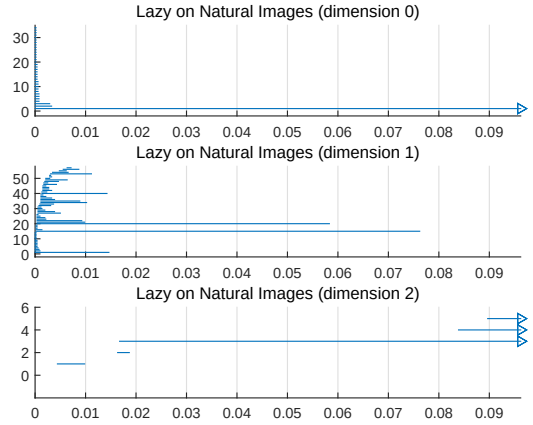

Fig. 13. PLEX result for $XP_8(200, 20)$

From the results of [5], we knew that the largest subspaces with the homology of the Klein bottle of 3×3, 4×4, 5×5, 6×6 and 7×7 patches are about 40%, 35%, 30% and 25% of points of X_3, X_4, X_5, X_6 and X_7 respectively. Combining the current results, we may conclude that the size of the largest subspace having the Klein bottle's homology of $n \times n$ patches depends on the patch size n, and the larger of patch size the smaller the size of the largest subspace. Hence it is necessary to discuss different sizes patches in natural images.

VII. Conclusion

In this paper we apply persistent homology to study natural image 8×8 and 9×9 patches, and obtain similar results to the papers [4], [5], the results of in this paper enlarge image analysis to larger patches. We find the largest subspaces of X_8 and X_9 with the Klein bottle's homology, and the size of the largest subspace of $n \times n$ natural image patches having the Klein bottle's homology is decreases as increasing of n. Thus we need only study $n \times n$ natural image patches for sufficiently

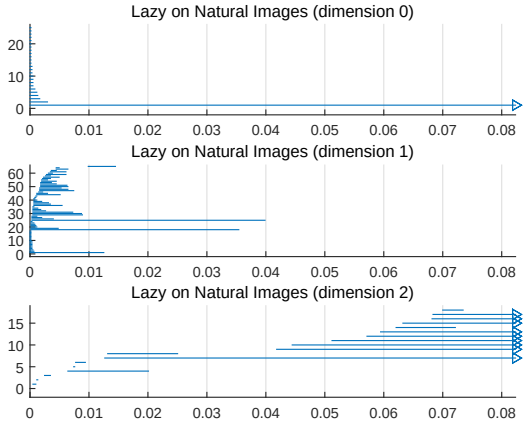

Fig. 14. PLEX result for $XP_8(200, 25)$

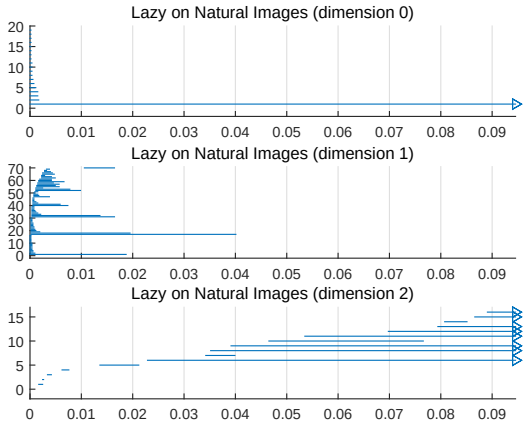

Fig. 15. PLEX result for $XP_8(200, 25)$

small n. The Klein bottle's feature of natural image patches may improve techniques of image compression [4], [6]. But it is worth to study that for how big of n, the $n \times n$ natural image patches have no the Klein bottle feature. As increasing of n, the computing for $n \times n$ patches becomes more difficult.

Acknowledgment

The authors are very grateful to the reviewers for their valuable comments and corrections.

The project is supported by the National Natural Science Foundation of China (Grant No.61471409).

References

[1] J. Huang, and D. Mumford, *Statistics of natural images and models.* In Proc. of IEEE Conf. on Computer Vision and Pattern Recognition, (1999), pp. 541–547.

[2] B.A. Olshausen, and D.J. Field, *Natural image statistics and efficient coding.* Network: Computation in Neural Systems, 7 2(1996), pp. 333–339.

[3] A. B. Lee, K. S. Pedersen, and D. Mumford, *The non-linear statistics of high-contrast patches in natural images.* Internat. J. Computer Vision, 54 1-3(2003), pp. 83–103.

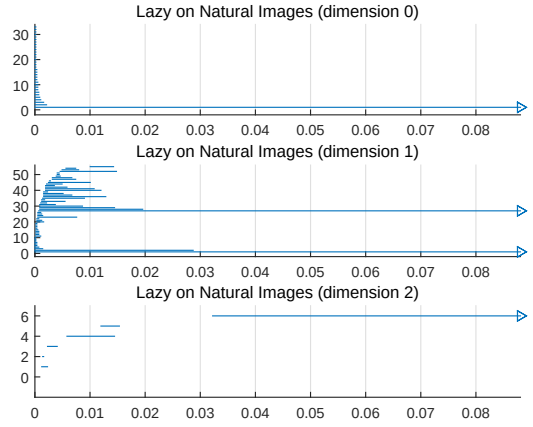

Fig. 16. PLEX result for $XP_9(200, 18)$

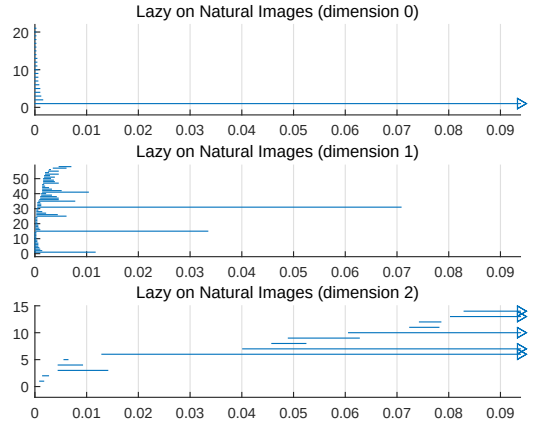

Fig. 17. PLEX result for $XP_9(200, 23)$

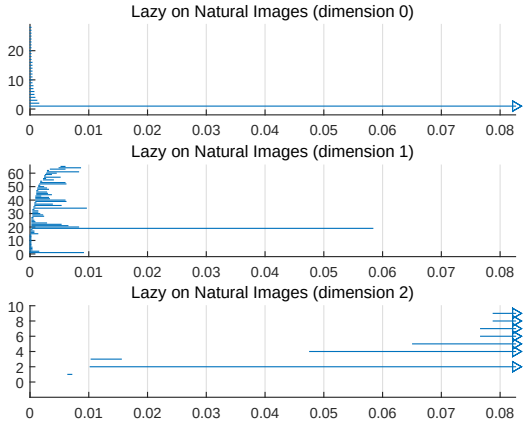

Fig. 18. PLEX result for $XP_9(200, 23)$

[4] G. Carlsson, T. Ishkhanov, V. de Silva, A. Zomorodian, *On the local behavior of spaces of natural images.* Internat. J. Computer Vision, 76 (2008), pp. 1–12.

[5] S. Xia, *A topological analysis of high-contrast patches in natural images.* J. Nonlinear Sci. Appl., 9 (2016), pp. 126–138.

[6] J. Perea and G. Carlsson *A Klein-Bottle-Based Dictionary for Texture Representation.* Internat. J. Computer Vision, 107 (2014), pp. 75–97.

[7] H. Jegou, M. Douze, and C. Schmid, *Hamming Embedding and Weak geometry consistency for large scale image search.* Proceedings of the 10th European conference on Computer vision, October, (2008), pp. 304–317.

[8] H. Adams and G. Carlsson, *On the nonlinear statistics of range image patches.* SIAM J. Imag. Sci., 2 (2009), pp. 110–117.

[9] H. Edelsbrunner, D. Letscher, and A. Zomorodian, *Topological persistence and simplification.* Discrete Comput. Geom., 28 4(2002), pp. 511–533.

[10] A. Zomorodian and G. Carlsson, *Computing Persistent Homology.* Discrete Comput. Geom., 33 (2005), pp. 249–274.

[11] V. de Silva and G. Carlsson, *Topological estimation using witness complexes.* Proc. Sympos. Point-Based Graphics, (2004), pp. 157–166.

[12] H. Adams and A. Tausz, *Javaplex tutorial.* http://javaplex. google-code.com/svn/trunk/reports /javaplex_tutorial/javaplex_tutorial.pdf.

[13] G. Carlsson, *Topology and data.* Bulletin (New Series) of the American Mathematical Society, 46 2(2009), pp. 255–308.